Electrical and optical properties of iron in GaN, AlN, and InN

Darshana Wickramaratne,[1,2] Jimmy-Xuan Shen,[3] Cyrus E. Dreyer,[4,5] Audrius Alkauskas,[6,7] and Chris G. Van de Walle[1]
[1]*Materials Department, University of California, Santa Barbara, Santa Barbara, California 93106-5050, USA*
[2]*Center for Computational Materials Science, United States Naval Research Laboratory, Washington, DC 20375, USA*
[3]*Department of Physics, University of California, Santa Barbara, Santa Barbara, California 93106-9530, USA*
[4]*Department of Physics and Astronomy, Stony Brook University, Stony Brook, New York 11794-3800, USA*
[5]*Center for Computational Quantum Physics, Flatiron Institute, 162 5th Avenue, New York, New York 10010, USA*
[6]*Center for Physical Sciences and Technology (FTMC), Vilnius LT-10257, Lithuania*
[7]*Department of Physics, Kaunas University of Technology, Kaunas LT-51368, Lithuania*

(Received 26 February 2019; published 14 May 2019)

Iron is a common trace impurity in the group-III nitrides. Iron is also intentionally introduced in III-nitride electronic devices to create semi-insulating substrates and in the context of spintronics and quantum information applications. Despite the wide-ranging consequences of iron's presence in III-nitrides, the properties of iron impurities in the nitrides are not fully established. We investigate the impact of iron impurities on the electrical and optical properties of GaN, AlN, and InN using first-principles calculations based on a hybrid functional. We report formation energies of substitutional and interstitial iron impurities as a function of the Fermi-level position. We also investigate complexes of Fe with substitutional oxygen on the nitrogen site, with nitrogen vacancies and with hydrogen interstitials. In GaN and AlN, iron on the cation site is amphoteric. We discuss the role of the Fe-induced acceptor level and its impact on nonradiative recombination in the context of loss mechanisms in light emitters, and current collapse in high-electron-mobility transistors. In InN, we find the iron interstitial to be the most favorable configuration, where it acts as a shallow double donor.

DOI: 10.1103/PhysRevB.99.205202

I. INTRODUCTION

The III-nitride semiconductors, GaN, AlN, InN and their alloys, are key materials for light-emitting diodes and lasers in the visible and ultraviolet spectrum [1] and are increasingly used in power electronics and high-electron-mobility transistors (HEMTs) [2]. Iron is sometimes *intentionally* introduced in the fabrication of nitride semiconductor devices, for instance, to create semi-insulating GaN buffer layers for HEMTs [3]. Transition-metal impurities in GaN or AlN are also being considered for spintronics applications [4–6] and as spin qubits for quantum-information technology applications [7].

The growth of nitride semiconductors can also result in the *unintentional* incorporation of iron. Contamination may arise from the presence of silica or alumina components in the system or from the reaction of amides and halides formed from gas sources with stainless steel components [8]. Memory effects following the intentional incorporation of iron can also lead to unintentional incorporation of iron in subsequent growth processes [9]. Secondary ion mass spectroscopy (SIMS) on bulk GaN samples grown using hydride vapor phase epitaxy (HVPE) [10,11] revealed the presence of iron incorporated unintentionally at concentrations of 10^{15} cm^{-3} [10]. The unintentional incorporation of iron in these samples was (at least partially) attributed to the Mg source used for *p*-type doping. Indeed, it has been demonstrated that incomplete purification of the organometallic precursors that are used as the Mg source for *p*-type doping can lead to the presence of iron [12], which could be unintentionally incorporated in the III-nitrides.

The use of iron to create semi-insulating GaN buffer layers for GaN/AlGaN HEMTs has also been associated with negative impacts on the performance of nitride HEMTs. In particular, current collapse in the drain-source current and shifts in the threshold voltage have been correlated with the concentration of iron in the GaN buffer [13]. Trace concentrations of iron have also been associated with efficiency losses in nitride optoelectronic devices. Time-resolved photoluminescence (TRPL) studies identified iron as an efficient Shockley-Read-Hall recombination center leading to nonradiative recombination lifetimes considered detrimental to the internal quantum efficiency (IQE) of light-emitting diodes (LEDs) [14,15].

Iron in AlN and InN has been studied less in comparison to GaN. Iron intentionally introduced in AlN was found to act as a deep acceptor [16] and leads to narrow emission lines with long luminescence lifetimes [17–20]. Such characteristics have been studied in detail in Fe-doped GaN and were associated with internal *d*-*d* transitions between different spin multiplet states [21]. Malguth *et al.* [21] used the position of the deep acceptor level due to Fe on the cation site in GaN and AlN [16] to determine the position of the Fe level in other III-V semiconductors based on theoretical band offsets. For InN, they found the acceptor level to lie above the InN conduction-band minimum (CBM), but the assessment was based on an incorrect band gap of 2 eV that was widely accepted at the time. The

actual position of the Fe acceptor level in InN is thus still uncertain.

When incorporated substitutionally into any of the III-nitrides, the iron d states split into a series of states due to a combination of the (approximately) tetrahedral crystal field and the exchange splitting. This gives rise to excited states which impact the electrical and optical properties. These excited states have been shown to lead to characteristic radiative optical transitions [21] and also to enable efficient nonradiative carrier capture processes [22,23].

Iron impurities in nitride semiconductors have been studied using first-principles calculations based on density functional theory (DFT). Prior work relied mostly on conventional functionals such as the local density approximation (LDA) or the generalized gradient approximation (GGA) [24–26]. Calculations at the LDA or GGA level have several shortcomings, including uncertainty in defect levels and formation energies due to the underestimation of the band gap [27], incorrect positioning of the valence-band maximum (VBM) on an absolute scale [28], and challenges in describing localized states such as transition-metal d states. GGA+U calculations [29] have been performed in an attempt to correct for this, but have failed to obtain good agreement with the experimental data for Fe in GaN. Hybrid functionals have been shown to provide much more accurate band structures as well as improved descriptions of localization [27]. Hybrid functional calculations for Mn in Ge [30] and in GaN [31] demonstrated excellent agreement with photoemission data, and for Fe in GaN the acceptor level was identified to be 0.5 eV below the GaN CBM [22,32], in agreement with absorption [21] and deep-level transient spectroscopy (DLTS) [33] measurements of Fe-doped GaN.

This overview of prior work makes clear that many aspects of iron impurities in nitrides remain to be explored. Here we report hybrid functional calculations of formation energies, thermodynamic transition levels, and optical transition levels due to iron as a substitutional and interstitial impurity in GaN, AlN, and InN. We consider Fe incorporation on the cation, anion, and interstitial sites of each nitride semiconductor. The incorporation of Fe as an acceptor can also lead to complexes with donors, for instance, with nitrogen vacancies [34]. Regarding complexes with impurities, we focus on elements that are often unintentionally incorporated during the growth of GaN, such as oxygen [35] or hydrogen [36].

Our systematic study shows that Fe can be stable in different configurations in the various III-nitrides. We show that Fe in GaN and AlN acts a deep acceptor in both materials and gives rise to broad free-to-bound optical transitions in the visible. In contrast, Fe in InN is stable in an interstitial configuration and acts as a shallow donor. Complexes give rise to optical transitions that are distinct from those due to the substitutional acceptor. Some of the results on Fe in GaN were previously reported [22]; they are repeated here in the interest of presenting a comprehensive picture of the behavior of Fe in III-nitrides but with significantly more detail.

In Sec. II we describe the computational methodology. In Secs. III A and III B we report on the electronic and optical properties of Fe incorporated substitutionally and interstitially in GaN. We also discuss the electronic and optical properties of Fe complexes in GaN in Secs. III C and III D. The role of Fe in GaN as an electron trap in III-nitride high-electron-mobility transistors and as an efficient recombination center is discussed in Secs. III E and III F. In Sec. IV we report on the electronic and optical properties of Fe in AlN, and the properties of Fe in InN are presented in Sec. V. General trends that can be inferred from our work are discussed in Sec. VI. Key results are summarized in Sec. VII.

II. METHODS

Our calculations are based on DFT using the hybrid functional of Heyd, Scuseria, and Ernzerhof (HSE) [37] as implemented in the Vienna Ab Initio Simulation Package (VASP) [38,39]. The mixing parameter for the Hartree-Fock potential is set to 0.25 for InN, 0.31 for GaN, and 0.33 for AlN [40], chosen to produce band gaps that are in good agreement with the experimental values for each material [41]. Our HSE-calculated band gaps are 0.68 eV for InN, 3.48 eV for GaN, and 6.18 eV for AlN; the corresponding experimental gaps are 0.70 eV for InN, 3.50 eV for GaN, and 6.19 eV for AlN [41]. Lattice parameters are also found to be within 1% of the experimental values for each material [41]. The interaction between the valence electrons and ionic cores is described within the projector augmented wave (PAW) approach [42] with a plane-wave energy cutoff of 400 eV. Ga d states and In d states were treated as part of the core.

Point-defect calculations were performed using a 96-atom supercell, and the Brillouin zone was sampled using a $(2 \times 2 \times 2)$ Monkhorst-Pack grid. Spin polarization was included in all cases. Spin configurations were calculated by enforcing the spin multiplicity. To determine the likelihood of incorporating an impurity in a crystal, we calculate the formation energy. For the example of Fe substituting on the Ga site in GaN, the formation energy is given by [27]

$$E^f\left(\mathrm{Fe}_{\mathrm{Ga}}^q\right) = E_{\mathrm{tot}}\left(\mathrm{Fe}_{\mathrm{Ga}}^q\right) - E_{\mathrm{tot}}(\mathrm{GaN}) + \mu_{\mathrm{Ga}} - \mu_{\mathrm{Fe}} + qE_F + \Delta^q\,, \tag{1}$$

where $E_{\mathrm{tot}}(\mathrm{GaN})$ is the total energy of the pristine GaN supercell, $E_{\mathrm{tot}}(\mathrm{Fe}_{\mathrm{Ga}}^q)$ is the total energy of the structure containing the impurity in charge state q, and μ_{Ga} and μ_{Fe} are the chemical potentials of Ga and Fe. μ_{Ga} can vary between Ga-rich (equilibrium with bulk Ga) and Ga-poor conditions (equilibrium with N_2 molecules). For μ_{Fe}, the upper limit is set by the solubility-limiting phase, Fe_3N. E_F is the Fermi level, which is referenced to the VBM (E_v), and Δ^q is the finite-size correction for charged defects [43,44]. For complexes containing oxygen, the chemical potential for O is set by the formation of Ga_2O_3 (which corresponds to the solubility limit).

For each defect or complex, we consider all possible charge states q. When dealing with transition-metal impurities, a different notation is often employed, reflecting the oxidation state of the impurity. For example, in the charge-state notation we refer to the neutral charge state of substitutional Fe as $\mathrm{Fe}_{\mathrm{Ga}}^0$, while in the oxidation-state notation it is referred to as Fe^{3+}. Similarly, the negative charge state $\mathrm{Fe}_{\mathrm{Ga}}^-$ would be referred to as Fe^{2+}, and the positive charge state $\mathrm{Fe}_{\mathrm{Ga}}^+$ as Fe^{4+}. Our discussion of computational results will consistently use the charge-state notation; we will only refer to the oxidation

state when comparing with experimental reports, which often use the oxidation-state terminology.

The thermodynamic transition level $\varepsilon(q/q')$ is defined as the Fermi-level position below which the defect is stable in the charge state q and above which it is stable in charge state q'. It is calculated as

$$\varepsilon(q/q') = \frac{E^f(D^q; E_F = 0) - E^f(D^{q'}; E_F = 0)}{q' - q}, \quad (2)$$

where $E^f(D^q; E_F = 0)$ is the formation energy of D^q when the Fermi level is at the VBM (i.e., for $E_F = 0$). The charge-state transition level (q/q') is thus determined by the Fermi-level position at which the formation energies of charge states q and q' are equal.

We will discuss optical transitions due to Fe and Fe-related complexes in the III-nitrides by constructing configuration-coordinate (CC) diagrams [45,46]. CC diagrams describe the change in energy as the atomic coordinates change for a given charge state of a defect. Since the atomic relaxations differ for different charge states, the peak energies in an absorption or luminescence process differ from the thermodynamic transition level [which gives the energy of the so-called zero phonon line (ZPL)]. To calculate the peak absorption and emission energies associated with a change in charge state from q to q' we use our definition for the charge-state transition level, $\varepsilon(q/q')$ [Eq. (2)] but keep the atomic configuration of the defect fixed: in the final state following the optical process the atomic configuration of the defect is the same as in the initial charge state.

For example, if we consider a photoluminescence process that involves the Fe_{Ga} acceptor level and a hole in the valence band, the peak photoluminescence (PL) energy E_{PL} can be calculated as

$$E_{PL} = \varepsilon(0/1-) - E_{rel}, \quad (3)$$

where $\varepsilon(0/-)$ is the charge-state transition level of the Fe_{Ga} acceptor referenced to the VBM of GaN and E_{rel} is the relaxation energy, i.e., the energy difference between Fe_{Ga} in the neutral charge state in the atomic configuration of the negative charge state and the energy of Fe_{Ga} in the neutral charge state in its equilibrium geometry. For optical transitions that involve the Fe_{Ga} acceptor level and an electron in the conduction band, the photoluminescence peak energy [Eq. (3)] can be calculated using the charge-state transition level, $\varepsilon(0/-)$, as $E_{PL} = E_g - \varepsilon(0/1-) - E_{rel}$, where E_g is the band gap of the material.

III. IRON IMPURITIES IN GaN

A. Electronic properties of Fe in GaN

Formation energies for various configurations of iron in GaN are shown in Fig. 1. Iron on the nitrogen site, Fe_N, has a (2+/+) level at E_v+2.73 eV. In the positive charge state, the four nearest-neighbor Ga atoms relax outward by 19% of the N-Ga bond length. In the $q = 2+$ charge state, there is an asymmetric outward relaxation of the four nearest-neighbor Ga atoms; the Fe-Ga bond lengths relax outward by 20% along the basal plane and by 29% along the axial direction.

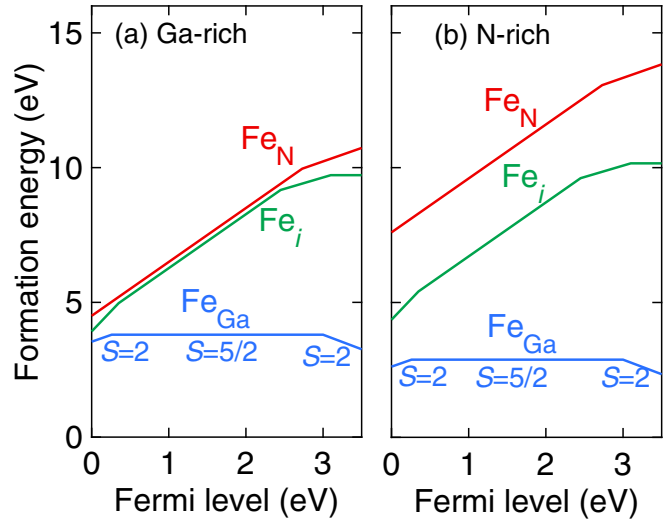

FIG. 1. Formation energy vs Fermi level for Fe_{Ga}, Fe_N, and Fe_i in GaN in different charge states under (a) Ga-rich conditions and (b) N-rich conditions. The slope of each line segment indicates the stable charge state of the defect at a particular Fermi level, and kinks in the curves correspond to charge-state transition levels [Eq. (2)]. For Fe_{Ga}, the spin multiplicity S is indicated for each of the charge states.

These large atomic relaxations can be explained by the large mismatch in ionic radii between N and Fe.

The iron interstitial Fe_i has a (3+/2+) level at E_v+0.35 eV, a (2+/+) level at E_v+2.45 eV, and a (+/0) level at E_v+3.05 eV. In the $q = 2+$ and $q = 3+$ charge states, Fe_i bonds to four nearest-neighbor nitrogen atoms. In the positive charge state, Fe_i bonds to a single nitrogen atom and the Ga atoms that are nearest neighbor to this N atom are displaced outwards by 3% of the Ga-N bond length.

Both Fe_N and Fe_i have very high formation energies, larger than the formation energy of Fe_{Ga} regardless of the position of E_F or the choice of chemical potential. Indeed, electron paramagnetic resonance (EPR) measurements on Fe-doped GaN have observed Fe substituted on the Ga site [47], consistent with our finding that Fe_{Ga} has the lowest formation energy.

The electronic properties of Fe substituted on the Ga site can be understood as follows. Removing one Ga atom from the GaN lattice creates four nitrogen dangling bonds that point towards the vacant Ga site. When a Fe atom is incorporated on this site, the tetrahedral environment (ignoring the slight breaking of symmetry in the wurtzite structure) splits the Fe d states into three t_2 states and two e states. The exchange splitting is large, which results in the majority spin states being pushed below the N p states and the minority states being pushed above the conduction-band minimum (CBM), as illustrated in Fig. 2. We find a peak in the occupied Fe d spin-up states at 7.7 eV below the VBM, as shown in the density of states in Fig. 3(a). The corresponding peak in the unoccupied spin-down states is located 0.8 eV above the CBM at Γ.

The neutral charge state, Fe^0_{Ga}, is a spin sextuplet ($S = 5/2$). This state is commonly referred to as Fe^{3+}, where the "3+" indicates the oxidation state. The lattice distortion

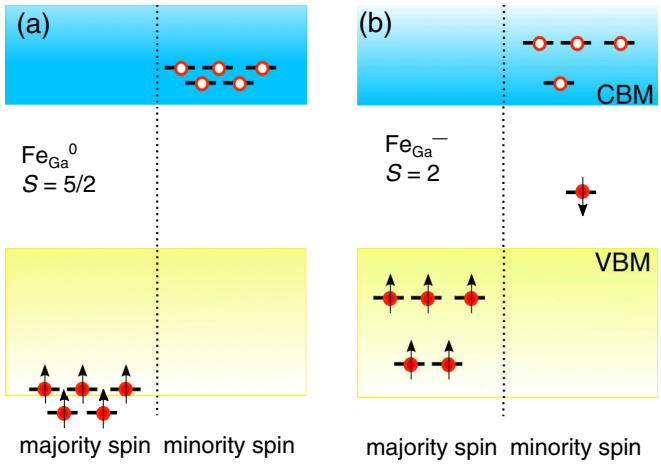

FIG. 2. Schematic illustration of the single-particle states for (a) neutral Fe_{Ga}^{0} and (b) negative Fe_{Ga}^{-} in GaN.

around Fe_{Ga}^{0} is small, with the four nearest-neighbor N atoms moving outwards by 0.5% of the Ga-N bond length. This indicates the Fe atom provides a good size match for the Ga atom it replaces. The negative charge state (Fe_{Ga}^{-}) (or

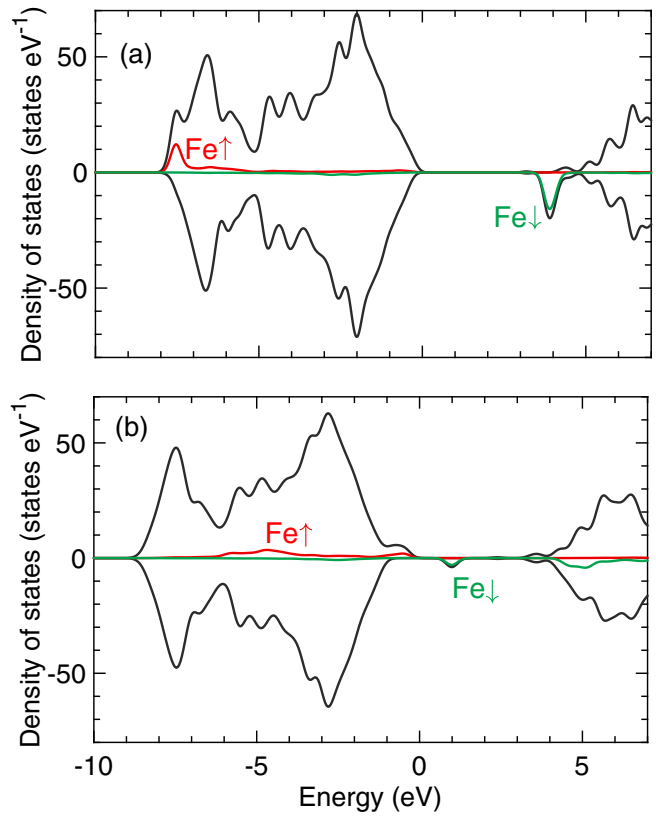

FIG. 3. Spin-polarized density of states for (a) neutral and (b) negative charge states of Fe_{Ga} in GaN. The majority spin density of states is shown along the positive vertical axis and the minority spin density of states along the negative vertical axis. The contributions of the Fe majority spin states are illustrated in red, and the Fe minority spin states are illustrated in green. The zero of energy is set at the valence-band maximum.

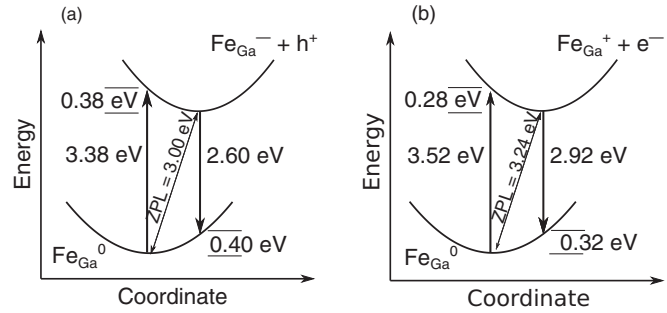

FIG. 4. Configuration-coordinate diagrams for the Fe_{Ga} impurity in GaN. (a) A transition between the $(0/-)$ acceptor level and a hole at the VBM leads to an absorption peak at 3.38 eV and emission at 2.60 eV. (b) A transition between the $(+/0)$ donor level and an electron at the CBM leads to an emission peak at 2.92 eV.

2+ oxidation state Fe^{2+}) is a spin quintuplet ($S = 2$). The four nearest-neighbor N atoms move outwards by 4%. One spin-down d state is now occupied and has moved into the gap. In the positive charge state, Fe_{Ga}^{+}, the N atoms relax inwards by 1.1%. The $(+/0)$ levels appear at 0.26 eV above the VBM. Consistent with prior reports [48,49], we find the wave function for the positive charge state localized on the Fe atom and the four nearest-neighbor nitrogen sites.

Figure 1 shows that the $(0/-)$ thermodynamic transition level (acceptor level) is located 0.50 eV below the CBM. This result is consistent with DLTS measurements [33] and with UV-VIS transmission spectra showing an onset in absorption at 2.86 eV in Fe-doped GaN [21]. Our results agree with previous hybrid functional calculations by Puzyrev *et al.* [32], who also found the $(0/-)$ thermodynamic transition level 0.5 eV below the CBM. However, they differ from the hybrid functional calculations of Alippi *et al.* [48], who found the $(0/-)$ due to Fe_{Ga} level to be 0.93 eV below the CBM. This difference may be related to their use of 25% mixing in the HSE calculations, which leads to a lower band gap of 3.33 eV, as well as a lesser degree of localization of d states.

B. Optical properties of Fe_{Ga} in GaN

1. Free-to-bound transitions

The optical transitions associated with the $(0/-)$ and $(+/0)$ transition levels of Fe_{Ga} are illustrated in Fig. 4. Related to the acceptor level [Fig. 4(a)], we find that optical absorption occurs in the process $Fe_{Ga}^{0} \rightarrow Fe_{Ga}^{-} + h^{+}$, with an onset at the ZPL of 3.00 eV and a peak at 3.38 eV. This is in agreement with experimental studies on GaN samples intentionally doped with iron, which reported an onset in absorption at 2.86 eV, with a peak at 3.27 eV [21]. The Fe_{Ga} can also give rise to emission, with the $Fe_{Ga}^{-} + h^{+} \rightarrow Fe_{Ga}^{0}$ process leading to blue emission with a peak at 2.60 eV.

The donor level close to the VBM also allows for optical transitions [Fig. 4(b)]. The $Fe_{Ga}^{+} + e^{-} \rightarrow Fe_{Ga}^{0}$ process gives rise to emission at 2.92 eV; the corresponding absorption process has a ZPL at 3.24 eV and would peak at above-band-gap energies.

Our results indicate that the presence of Fe_{Ga} can lead to blue or violet emission. Photoluminescence measurements

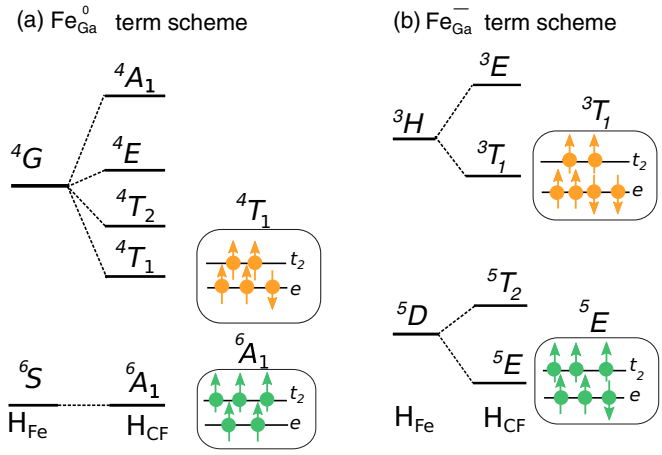

FIG. 5. Schematic illustration of the term schemes for ground and excited states of (a) Fe^0_{Ga} and (b) Fe^-_{Ga}. The symbols for the energy levels correspond to Fe in a tetrahedral crystal field; deviations due to the wurtzite crystal field are minor. Representative orderings of majority (↑) and minority (↓) spin states are illustrated for the ground state (green) and first low-spin excited state (orange) of each charge state within the boxes next to the respective energy level.

of Fe-doped GaN with above-band-gap excitation indeed observed a broad PL peak at 2.96 [14] or 2.80 eV [50]. This emission energy is close to the 2.92 eV we predict for the $Fe^+_{Ga} + e^- \rightarrow Fe^0_{Ga}$ process [Fig. 4(b)]. Alternatively, it could arise from a $Fe^-_{Ga} + h^+ \rightarrow Fe^0_{Ga}$ process [Fig. 4(a)], which we predict to have an emission peak at 2.60 eV—additional discussion about this emission is included in Sec. III F. As to the difference between the experimentally observed emission peaks (2.96 eV in Ref. [14] and 2.80 eV in Ref. [50]), this could potentially indicate formation of a Fe_{Ga}-related complex (see Sec. III D).

2. *Internal transitions*

The *d* states of Fe when substituted on a Ga site are subject to a tetrahedral crystal field (with slight deviations due to the wurtzite crystal symmetry). Within a tetrahedral crystal field, the Fe 3*d* states are split into *e* and t_2 states. In addition, exchange splits these states into spin-up and spin-down states (Fig. 2). The combination of the tetrahedral crystal field and exchange splitting gives rise to a series of excited states of the Fe *d* states in the Fe^0_{Ga} and Fe^-_{Ga} charge states. The term scheme showing the relative energy differences between the ground state and excited states of Fe^0_{Ga} and Fe^-_{Ga} is illustrated in Fig. 5. For the quadruplet excited states of Fe^0_{Ga}, we use the ordering of states proposed by Neuschl *et al.* [51], that is, $^4T_1$, ^4E, $^4T_2$, and $^4A_1$. For the excited states of Fe^-_{Ga}, we use the ordering of lowest energy states proposed by Malguth *et al.* [21], that is, ^5E, $^5T_2$, $^3T_1$, and ^3E. For the $^6A_1$ ground state and $^4T_1$ excited state of Fe^0_{Ga} and the ^5E ground state and $^3T_1$ excited state of Fe^-_{Ga}, we illustrate the majority and minority spin states in the *e* and t_2 states.

Photoluminescence measurements [8,21,52] of Fe in GaN have observed a narrow emission line at 1.299 eV which was assigned to an internal transition between the $^4T_1$ excited state and the $^6A_1$ ground state of Fe^0_{Ga}. This emission line has only been observed in measurements that relied on 2.41-eV–subband-gap excitation [21]; this is important to prevent photoexcited electrons and holes from being present simultaneously, which would lead to nonradiative recombination at a much faster rate than the radiative recombination (see Sec. III F). Low-temperature time-resolved luminescence measurements of this emission line find it to have a long lifetime of 8 ms [53], which is consistent with the spin flip required to transition from the $^4T_1$ excited state to the $^6A_1$ ground state.

We can use a Δ self-consistent-field (ΔSCF) [54] approach to determine the energies between the ground state ($S = 5/2$) and the first quadruplet ($S = 3/2$) excited state of Fe^0_{Ga}. Our HSE calculations result in an energy difference of 1.55 eV [22]. While this is slightly larger than the experimental value, it still indicates that HSE can be used to predict excited-state energies. As documented in Ref. [22], further confirmation was provided by calculations using the random phase approximation (RPA) that used the geometries obtained with HSE. RPA yielded an energy difference of 1.40 eV between the ground state and the first excited state. We have also investigated the influence of the atomic geometry on the excited-state energies and find the energies to be insensitive to the details of the atomic structure. If the $S = 3/2$ excited state is calculated in the geometry of the $S = 5/2$ ground state, the energy difference between the ground state and the first excited state is 1.35 eV, differing by only 50 meV from the result obtained for separately optimized geometries. We note that, in general, a description of spin multiplet states requires going beyond the Kohn-Sham picture, since wave functions composed of more than one Slater determinant may be needed [55].

C. Electronic properties of Fe_{Ga} complexes in GaN

Thus far we have focused on the properties of isolated Fe impurities in GaN. We now investigate the possibility of complex formation, focusing on Fe_{Ga}, which is the lowest energy configuration for the Fe impurity. Since Fe_{Ga} behaves as a deep acceptor when the Fermi level is high in the gap, we expect complexes could be formed with deep or shallow donors, as was suggested in studies based on EPR and Zeeman spectroscopy [47,56]. We will consider complexes with oxygen on the nitrogen site, O_N, with interstitial hydrogen, H_i, and with the nitrogen vacancy, V_N.

A recent computational investigation by Puzyrev *et al.* [32] examined such complexes and found large binding energies [32]; however, they did not report formation energies and hence did not address the likelihood of such complexes being actually present in the material. In Fig. 6 we summarize our calculations of the formation energies of Fe_{Ga} complexes.

All of the complexes give rise to deep levels within the GaN band gap. Fe_{Ga}-H_i is a deep donor with a (+/0) level at E_v +2.07 eV, in agreement with Ref. [32]. In the neutral charge state of Fe_{Ga}-H_i the Fe-H bond length is 1.88 Å while in the positive charge state H_i is in an antibonding configuration, bonding to a N atom along the extension of a Fe-N bond. For the Fe_{Ga}-V_N complex, we find a (0/−) level 0.37 eV below the CBM, also in agreement with Ref. [32]. In the neutral charge state, the Fe-N bond length between Fe

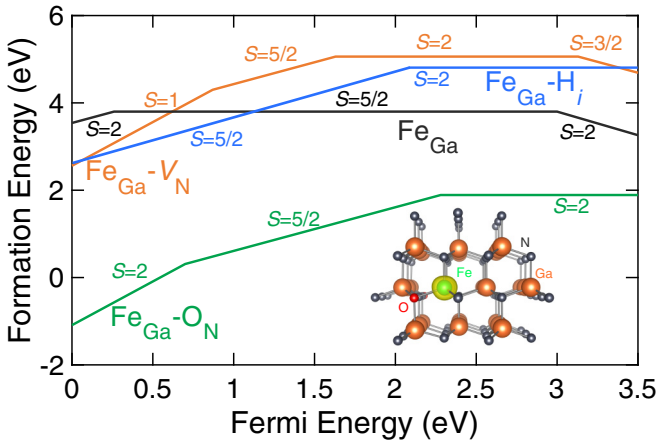

FIG. 6. Formation energy vs Fermi level for Fe complexes with H_i, O_N, and V_N in GaN under Ga-rich conditions. The formation energy of Fe_{Ga} is included for comparison. The spin multiplicity is listed next to each charge state for Fe_{Ga} and its complexes. The spin density of the positive charge state of the Fe_{Ga}-O_N complex is illustrated in the inset.

and the three nearest-neighbor N atoms is 6% larger than the Ga-N bond length, while in the − charge state the Fe-N bond lengths are 9% larger than the Ga-N bond length. We also find the Fe_{Ga}-V_N complex exhibits a (+/0) level at E_v +1.63 eV and a (2+/+) level at E_v +0.87 eV. In the + and 2+ charge states, the Fe-N bond length is 1.1% shorter than the Ga-N bond length.

Fe_{Ga}-O_N is the most stable among the complexes; its structure is illustrated in the inset of Fig. 6. It behaves as a deep donor with a (2+/+) transition level at E_v +0.70 eV and a (+/0) level at E_v +2.28 eV. In the neutral charge state we find the three nearest-neighbor N atoms move outwards by 1% of the Ga-N bond length and the Fe-O bond length is 12% larger than the Ga-N bond length. In the + and 2+ charge states the three nearest-neighbor N atoms move inwards by 1% and the Fe-O bond length is 4% larger than the Ga-N bond length.

In order to assess the stability of the complexes with respect to the constituent defects we determine their binding energies. For example, the binding energy E_b of the Fe_{Ga}-O_N complex in the neutral charge state is

$$E_b[(Fe_{Ga}\text{-}O_N)^0] = -E^f(Fe_{Ga}\text{-}O_N) + E^f(Fe_{Ga}^-) + E^f(O_N^+)\,, \tag{4}$$

resulting in a value $E_b = 2.98$ eV. Similarly, the binding energy of $(Fe_{Ga}\text{-}H_i)^0$ with respect to Fe_{Ga}^- and H_i^+ is 1.41 eV, and the calculated binding energy for $(Fe_{Ga}\text{-}V_N)^0$ with respect to Fe_{Ga}^- and V_N^+ is 1.50 eV.

Among the complexes we have studied, Fe_{Ga}-O_N exhibits the lowest formation energy for all values of the Fermi level within the GaN band gap. The formation energy of Fe_{Ga}-O_N is lower than the Fe_{Ga} impurity and is particularly low when the Fermi level is in the lower part of the band gap, due to the donor nature of the complex. In contrast, Fe_{Ga}-H_i and Fe_{Ga}-V_N exhibit significantly higher formation energies, larger than the formation energy of the isolated Fe_{Ga} defect; it is thus unlikely for these complexes to be incorporated at concentrations that are comparable to Fe_{Ga}, under either Ga-rich or N-rich conditions.

Our results about the stability and electrical behavior of the Fe_{Ga}-O_N complex are in agreement with experimental observations by Muret *et al.* [57]. Using deep-level optical spectroscopy (DLOS) studies on Fe-doped GaN grown by metallorganic vapor-phase epitaxy (MOVPE), they reported a donor level with an activation energy 1.39 eV below the GaN CBM [57]. The samples also contained high concentrations of unintentionally incorporated oxygen (as detected by SIMS [57]), rendering it likely for stable Fe_{Ga}-O_N complexes to form. The observed donor level is consistent with the (+/0) level of Fe_{Ga}-O_N that we calculate at 1.22 eV below the GaN CBM (Fig. 6).

Prior first-principles investigations of Fe incorporation in GaN have also assessed the formation of Fe clusters in GaN [58,59] by comparing differences in total energy between Fe_{Ga} dimers and trimers in different collinear spin configurations within GGA or GGA+U supercell calculations. We have compared the total energy of a neutral Fe_{Ga}-Fe_{Ga} dimer in a ferromagnetic and antiferromagnetic configuration; in such a complex, the Fe atoms are second-nearest neighbors. We find the antiferromagnetic configuration to be the ground state and lower in energy by 1 eV/Fe atom compared to the ferromagnetic configuration. This is in agreement with prior results that investigated the magnetic configuration of Fe_{Ga}-Fe_{Ga} dimers [58]. However, we find the formation energy of the Fe_{Ga}-Fe_{Ga} dimer in the neutral charge state to be very high (9.58 eV under Ga-rich conditions), and we find there is no binding between the Fe_{Ga} atoms in this complex. This makes it unlikely that these dimers would occur in any appreciable concentration.

We have also considered the properties of Fe_{Ga}-Fe_N dimers, in which Fe on the N site is now a nearest neighbor to Fe on the Ga site. Again we found the antiferromagnetic configuration to be lower in energy. The formation energy (under Ga-rich conditions) of the Fe_{Ga}-Fe_N complex in the neutral charge state is 11.64 eV; in the positive charge state, the formation energy is 9.03 eV when the Fermi level is at the VBM. This high formation energy again makes it unlikely that Fe_{Ga}-Fe_N dimers would play any role in Fe-containing samples.

D. Optical properties of Fe_{Ga} complexes in GaN

1. Free-to-bound transitions

The complexes also lead to a number of interesting optical transitions, as illustrated in Fig. 7. We focus here on transitions involving carriers at either the VBM or CBM and with energies in the visible or near-IR; transitions at lower energies are more likely to involve nonradiative recombination. We find that transitions between defect levels of Fe_{Ga} or its complexes and either the CBM or the VBM are allowed, i.e., they have sizable optical dipole matrix elements. For transitions involving the VBM, this is not surprising, since the Fe_{Ga} states have d character and the VBM has mainly N p character. For transitions involving the CBM, one might expect optical transitions to be weak since the conduction band mainly has Ga s character and the defect states are composed of the d states of iron. However, significant hybridization occurs between the Fe d states and the nearest-neighbor N p states,

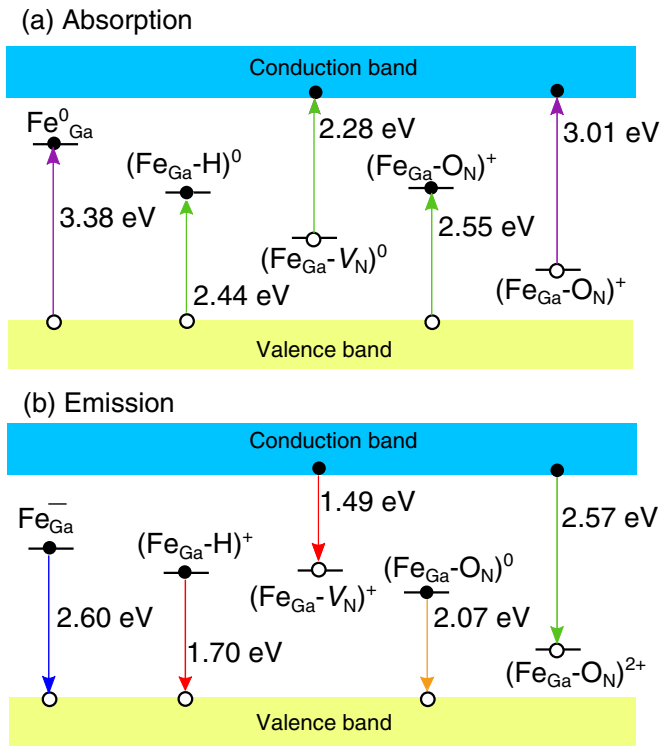

FIG. 7. Peak energies for (a) absorption and (b) emission processes due to Fe_{Ga} and its complexes with H_i, V_N, and O_N. The initial charge state for each optical transition is indicated. The color of each arrow corresponds to the color involved in the optical transition.

and with O p states in the case of the Fe_{Ga}-O_N complex. In addition, in GaN the CBM also has a significant amount of N p character. As a result, dipole matrix elements between the CBM and Fe_{Ga} or its complexes have a sizable magnitude and lead to allowed transitions. The hybridization appears to be stronger in the complexes: for isolated Fe_{Ga}, the dipole matrix element between the CBM and the Fe_{Ga} level is an order of magnitude smaller than the matrix element involving the VBM, while for the complexes the matrix elements for transitions with the CBM and with the VBM have comparable magnitudes.

For Fe_{Ga}-H_i complexes, radiative transitions between the $(+/0)$ of Fe_{Ga}-H_i and holes in the VBM would result in absorption that peaks at 2.44 eV and emission that peaks at 1.70 eV. Optical transitions between electrons at the CBM and the Fe_{Ga}-H_i $(+/0)$ level would result in absorption that peaks at 1.87 eV and emission that peaks at 1.05 eV, with a ZPL at 1.41 eV. Radiative transitions between the $(+/0)$ level of Fe_{Ga}-V_N and the CBM lead to an absorption process that peaks at 2.28 eV and emission that peaks at 1.49 eV, with a ZPL at 1.87 eV. For the Fe_{Ga}-O_N complex, finally, in Fig. 7 we considered radiative transitions between the valence band and the $(+/0)$ level of Fe_{Ga}-O_N; these would result in an absorption peak at 2.55 eV and emission that peaks at 2.07 eV, with a ZPL at 2.28 eV. We also considered radiative transitions between the conduction band and the $(+/0)$ level of Fe_{Ga}-O_N and find that this leads to an absorption process that peaks at 1.43 eV and to luminescence that peaks at 0.94 eV, with a relaxation energy of 0.28 eV and a ZPL of 1.22 eV. Radiative transitions can also occur between the $(2+/+)$ level of Fe_{Ga}-O_N. We find that transitions involving this level and the CBM lead to an absorption peak at 3.01 eV and emission that peaks at 2.57 eV, with a ZPL of 2.79 eV. If we consider radiative transitions between the $(0/-)$ level of Fe_{Ga}-V_N and the valence band, this would lead to absorption that peaks at 1.93 eV and luminescence that peaks at 1.23 eV.

2. Internal transitions

Due to the presence of the donor in the complex, the ground-state spin configurations of the Fe_{Ga} complexes in their various charge states differ from the spin configurations of Fe_{Ga} in the same charge state. Identifying the spin state of the stable charge states of the Fe complexes can be helpful for spectroscopic techniques that can identify the multiplicity of a defect charge state, such as electron spin resonance or Zeeman photoluminescence. Zeeman PL measurements on Fe-doped GaN identified a ZPL at 1.268 eV that did not have the d^5 structure associated with Fe^0_{Ga} [56]. The identification of a different spin configuration associated with this internal transition led to the conclusion that the line at 1.268 eV was due to an internal transition that involved an Fe_{Ga} complex rather than the Fe_{Ga} defect itself. Figure 6 shows that in the neutral charge state the complexes are all stable as a spin quintuplet ($S = 2$), which is the ground-state spin configuration of Fe_{Ga} in the negative charge state [see Fig. 5(b)]. The first excited state is again a low-spin configuration (in this case $S = 1$), and it is of interest to examine the energy difference with the $S = 2$ ground state.

Using HSE ΔSCF calculations, we find the $S = 1$ excited state of Fe_{Ga}-O_N to be 1.36 eV higher in energy than the $S = 2$ ground state. This value is lower than the ΔSCF energy we calculated for Fe_{Ga} (1.55 eV). Similarly, we find the $S = 1$ excited state of Fe_{Ga}-V_N to be 1.41 eV higher in energy than the $S = 2$ ground state. This trend of the excited-state energy for a Fe_{Ga}-related complex to be lower than the energy for Fe_{Ga} is consistent with the assignment of the ZPL at 1.268 eV to a Fe_{Ga}-related complex, being lower than the ZPL at 1.299 eV associated with Fe_{Ga}.

Among the various Fe_{Ga}-related complexes, Fe_{Ga}-O_N has the lowest formation energy as well as the largest binding energy. Therefore it is plausible that Fe_{Ga}-O_N complexes in the neutral charge state are the source of the ZPL at 1.268 eV observed in Fe-doped GaN [56], although we cannot really exclude other complexes.

E. Role of Fe in carrier trapping processes

AlGaN/GaN HEMTs commonly exhibit current collapse in the drain-source current (otherwise referred to as dispersion) and shifts in the threshold voltage [13,60]. The current collapse has been attributed to the presence of a deep acceptor in the GaN buffer of the HEMTs. Cho *et al.* [61] attributed this defect level, which occurs at ∼0.6 eV below the CBM of GaN, to nitrogen antisites. We feel this is unlikely, given that nitrogen antisites have very high formation energies and are thus not expected to be present [62].

Other measurements have observed a direct correlation between current collapse in nitride HEMTs and the presence of iron in the GaN buffer [60]. Indeed, iron is a likely

candidate because it is often intentionally introduced into the GaN buffer of nitride HEMTs to overcome the unintentional n-type conductivity in GaN due to background donors and achieve semi-insulating material. SIMS measurements identified the unintentional incorporation of Fe in the unintentionally doped (UID) GaN region of III-nitride HEMTs [13,60]. The proximity of the two-dimensional electron gas (2DEG) to the Fe that is unintentionally incorporated in the UID region can lead to nonradiative trapping of electrons from the 2DEG into the UID GaN region. Dynamic transconductance measurements by Silvestri *et al.* [60] on GaN/AlGaN HEMTs containing Fe-doped GaN buffers were used to determine the magnitude of current collapse; they indeed found a greater degree of current collapse as the concentration of the Fe in the buffer increased. The impact of iron on current collapse has also been corroborated by Meneghini *et al.* [63] using pulsed current-voltage measurements, which identified a trap with an activation energy of 0.60 eV with respect to the GaN CBM, and again correlated the current collapse with the Fe concentration in the GaN buffer.

The activation energy extracted from these studies agrees well with our calculations of the $(0/-)$ acceptor level due to Fe_{Ga} in GaN. However, there has been some debate over the Fe-related configuration that gives rise to the current collapse. Puzyrev *et al.* [32] and Mukherjee *et al.* [64] proposed Fe_{Ga}-V_N complexes as the source of current collapse in III-nitride HEMTs. They found that Fe_{Ga}-V_N gives rise to a level 0.5 eV below the GaN CBM [32]. They also investigated the role of hydrogen; for the hydrogenated Fe_{Ga}-V_N-H_i complex they calculated a level 1.5 eV below the GaN CBM. They noted that this is consistent with transient capacitance measurements on III-nitride HEMTs, where the $E_c - 0.5$ eV level is observed prehydrogenation but not posthydrogenation [65]. Mukherjee *et al.* [64] then proposed that hot carriers in III-nitride HEMTs can lead to dehydrogenation of Fe_{Ga}-V_N-H_i complexes and thus activate the Fe_{Ga}-V_N complex.

We find the Fe_{Ga}-V_N acceptor level at $E_c - 0.37$ eV below the GaN CBM (cf. Fig. 6) to be in reasonable agreement with the results of Puzyrev *et al.* [32]. However, our calculations show that the formation energy of Fe_{Ga}-V_N is very high, suggesting that Fe_{Ga}-V_N is unlikely to form. In addition, our calculations for the Fe_{Ga}-V_N-H_i indicate this also has a very high formation energy (6.21 eV in the neutral charge state). Puzyrev *et al.* [32] did not calculate these formation energies, and therefore they were unable to assess whether these complexes would actually form.

Instead of invoking complexes, we suggest that the Fe_{Ga} acceptor itself is the cause of current collapse. The calculated acceptor level, at $E_c - 0.5$ eV, is consistent with the experimental observations. We have previously shown [22] that the Fe_{Ga} acceptor level 0.5 eV below the GaN CBM acts as an efficient electron trap with a large electron capture coefficient, $\sim 10^{-8}$ cm^3 s^{-1}. In addition, hydrogenation would also deactivate the Fe_{Ga} acceptor, consistent with the observed deactivation of the $E_c - 0.6$ eV level upon hydrogenation [65]: Fig. 6 shows that the Fe_{Ga}-H_i complex has a $(0/+)$ level 2.07 eV above the VBM and thus hydrogenation would effectively suppress current collapse. We conclude that the Fe_{Ga} acceptor is the most likely source for the observed current collapse observed in nitride HEMTs.

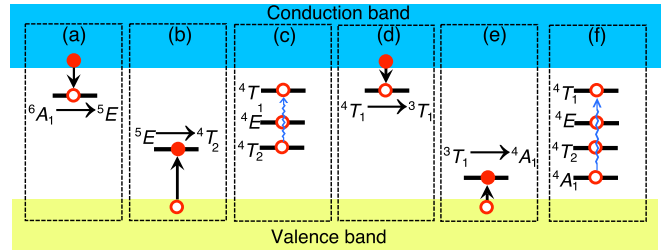

FIG. 8. Shockley-Read-Hall recombination cycle for electron and hole capture at Fe_{Ga}. (a) Electron capture into the $^6A_1/^5E$ level; (b) hole capture into the $^5E/^4T_2$ level; (c) intradefect relaxation between $^4T_2$ and $^4T_1$; (d) electron capture into the $^4T_1/^3T_1$ level; (e) hole capture into the $^3T_1/^4A_1$ level; and (f) intradefect relaxation between $^4A_1$ and $^4T_1$. After this last step processes (d)–(f) continue to repeat. The group theory symbols correspond to the Fe $3d$ states in tetrahedral symmetry. The ordering of the different ground and excited states is illustrated in Fig. 5.

F. Role of Fe in Shockley-Read-Hall recombination

Iron in GaN was recently shown to act as an efficient Shockley-Read-Hall recombination center [14]. This high rate of nonradiative recombination was surprising, given the position of the Fe_{Ga} acceptor level within the band gap, at 0.5 eV from the GaN CBM. Since capture rates decrease roughly exponentially as a function of energy difference with the band edge [66], the position of the acceptor level would indicate electron capture would be very fast but hole capture should be slow, and thus the overall Shockley-Read-Hall recombination rate would be low.

This seeming contradiction can be resolved by taking the excited states of Fe^0_{Ga} and Fe^-_{Ga} into account (cf. Fig. 5). This leads to new recombination pathways through which the efficient capture of both electrons and holes can occur. The recombination cycle is initialized in the ground state of Fe^0_{Ga} and then proceeds via the excited states of Fe^0_{Ga} and Fe^-_{Ga}, as illustrated schematically in Fig. 8. The calculated [22] electron and hole capture coefficients associated with the processes illustrated in Figs. 8(d) and 8(e) are large, on the order of 10^{-8} cm^3 s^{-1}. These capture coefficients are consistent with the electron and hole capture coefficients extracted from experiment in Ref. [14].

The efficient nonradiative processes associated with Fe in GaN also influences the optical properties. Photoluminescence measurements that relied on above-band-gap excitation [14,50] have not observed emission at 2.6 eV. Under conditions where both electrons and holes are created by photoexcitation, we saw that a very efficient nonradiative recombination occurs: holes are captured nonradiatively by an excited state of Fe^-_{Ga}, rather than in a radiative process that would lead to 2.6-eV emission. We find that the *radiative* capture coefficient for holes into Fe^-_{Ga} is low, less than 10^{-13} cm^3 s^{-1}. In contrast, nonradiative hole capture into the $^3T_1/^4A_1$ level [the process illustrated in Fig. 8(e)] is very fast. Our calculations show that the barrier for this hole capture process is low [Fig. 9(a)]. This leads to hole capture coefficients that are large and independent of temperature across a wide temperature range, as shown in Fig. 9(b).

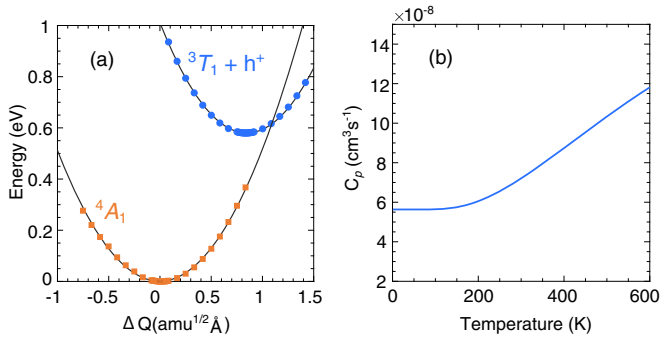

FIG. 9. (a) Calculated configuration-coordinate diagram for hole capture at the $^3T_1/^4A_1$ level. Symbols: calculated values; solid line: parabolic fit. The defect in the negative charge state ($^3T_1$) captures a hole and becomes neutral ($^4A_1$). (b) Nonradiative hole capture coefficient vs temperature into the $^3T_1/^4A_1$ level [cf. Fig. 8(e)].

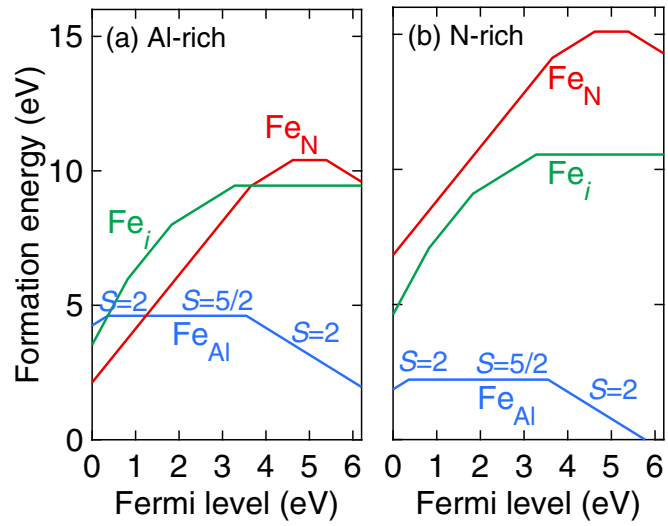

FIG. 10. Formation energy vs Fermi level for Fe_{Al}, Fe_N, and Fe_i in AlN in different charge states under (a) Al-rich conditions and (b) N-rich conditions. For Fe_{Al}, the spin multiplicity S is indicated for each of the charge states.

Hence, for photoluminescence measurements conducted with above-band-gap excitation at low temperatures [50] or room temperature [14], we expect nonradiative hole capture processes to be more efficient than radiative hole capture processes. Once this efficient nonradiative recombination cycle is initiated with the presence of electrons *and* holes, holes in the VBM will be captured nonradiatively into the $^3T_1/^4A_1$ level [cf. Fig. 8(e)] at a rate that is significantly faster than the radiative capture rate into the $^6A_1/^5E$ level that would lead to emission at 2.6 eV [cf. Fig. 4(a)].

These efficient nonradiative processes would also compete with the narrow emission at 1.299 eV, as discussed in Sec. III B 2. This radiative transition between the $^4T_1$ excited state and $^6A_1$ ground state of Fe^0_{Ga} has been observed in Fe-doped GaN excited by subband-gap light [8,21,52], with a lifetime of 8 ms [53]. Note that if above-band-gap excitation were used, the presence of both electrons and holes would lead to these carriers recombining nonradiatively via the excited states of Fe_{Ga}, which would greatly suppress the intensity of the emission of the internal transition.

IV. IRON IMPURITIES IN AlN

A. Electronic properties of Fe in AlN

In Fig. 10 we illustrate the formation energies of Fe_{Al}, Fe_N, and Fe_i in AlN as a function of Fermi-level position under Al-rich and N-rich conditions. The wider band gap of AlN allows additional charge states to be stable. Fe_N can occur in the 2+, +, 0, and − charge states. In each case we find a strong asymmetric outward relaxation of the nearest-neighbor Al atoms. In the 2+ and + charge states the Al atoms are displaced outwards by 21% of the Al-N bond length along the planar direction and 17% along the axial direction. In the neutral charge state the Al atoms are displaced outwards by 21% of the Al-N bond length along the planar direction and 14% along the axial direction. In the negative charge state we find the nearest-neighbor Al atoms to be displaced outwards by 18% along the planar direction and 20% along the axial direction. When incorporated as an interstitial in AlN, Fe_i acts as a deep donor and is stable in the 2+, +, and 0 charge states.

The formation energies of Fe_i and Fe_N can be modest when the Fermi level is close to the valence band, but since AlN is very difficult to dope *p* type [67], such conditions are unlikely to occur. For higher values of the Fermi level, the formation energies of Fe_i and Fe_N are high and hence Fe is unlikely to be incorporated in interstitial positions or substituting on the N site. Substitutional Fe on the Al site, Fe_{Al}, is thus the most likely configuration to occur, and the formation energy is particularly low under N-rich conditions and when the Fermi level is high in the gap. This is consistent with Mössbauer spectroscopy on Fe-doped AlN [68], where Fe was found to substitute on the Al site.

Similar to Fe_{Ga} in GaN, Fe_{Al} acts as a deep acceptor but with a (0/−) level at 2.65 eV below the AlN CBM. The incorporation of Fe on the Al site in the neutral charge state results in an outward relaxation of the nearest-neighbor nitrogen atoms by 2.6%, referenced to the equilibrium Al-N bond length. As illustrated in Fig. 11, we find the occupied Fe *d* spin-up states to be located below the AlN valence band at an energy roughly 7.1 eV below the VBM. The unoccupied spin-down states are in the AlN band gap, 4.3 eV above the AlN VBM. In the negative charge state, the nearest-neighbor nitrogen atoms relax outwards by 8.7%. We also find the positive charge state, Fe^+_{Al}, to be stable within the AlN band gap, with a (+/0) level at E_v+0.36 eV. In the positive charge state, the nearest-neighbor nitrogen atoms relax outwards by 1.76%.

Fe_{Al} occurs in high-spin configurations in the neutral and negative charge state. In its neutral charge state, Fe^0_{Al} is a spin sextuplet ($S = 5/2$), while in the negative charge state, Fe^-_{Al} is a spin quintuplet ($S = 2$). The spin quintuplet ground state of Fe^-_{Al} is consistent with EPR measurements of Fe-doped AlN [69].

B. Optical properties of Fe_{Al} in AlN

We illustrate the optical transitions due to the (0/−) level of Fe_{Al} in AlN in Fig. 12. Transitions involving a hole at the VBM [Fig. 12(a)] result in an absorption peak at 3.91 eV

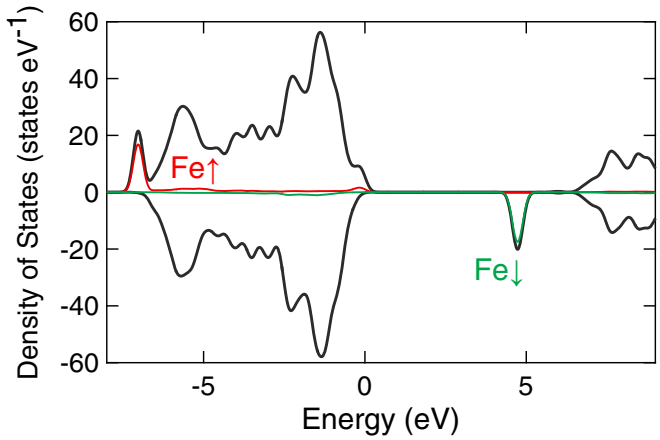

FIG. 11. Spin-polarized density of states for neutral Fe^0_{Al} in AlN. The majority spin density of states is shown along the positive vertical axis and the minority spin density of states along the negative vertical axis. The contributions of the Fe majority spin states are illustrated in red and the Fe minority spin states are illustrated in green. The zero of energy is at the VBM.

and an emission peak at 3.14 eV, with a ZPL of 3.55 eV. A transition involving an electron at the CBM [Fig. 12(b)] would give rise to yellow emission that peaks at 2.14 eV. Optical transitions between the $(+/0)$ level of Fe_{Al} and an electron at the CBM (not illustrated) would lead to absorption that peaks at 3.86 eV and emission that peaks at 2.90 eV.

When incorporated on the Al site in AlN, the d states of Fe are split due to a combination of the crystal field and exchange. Since Fe_{Al} is also tetrahedrally coordinated by four nitrogen atoms and experiences a qualitatively similar crystal field as Fe_{Ga}, Fe_{Al} in the neutral charge state has the same sextuplet spin multiplicity as Fe^0_{Ga}. We thus expect a similar sequence of excited states as has been found for Fe^0_{Ga} [cf. Fig. 5(a)]. We applied our ΔSCF approach to Fe^0_{Al} and find the energy difference between the sextuplet ($S = 5/2$) ground state and the quadruplet ($S = 3/2$) excited state to be 1.58 eV; within our error bar, this value is very similar to our calculated value for Fe^0_{Ga} in GaN. A study by Baur *et al.* [8] identified a narrow luminescence band at 1.297 eV that was attributed to the internal transition between the ground state and the first

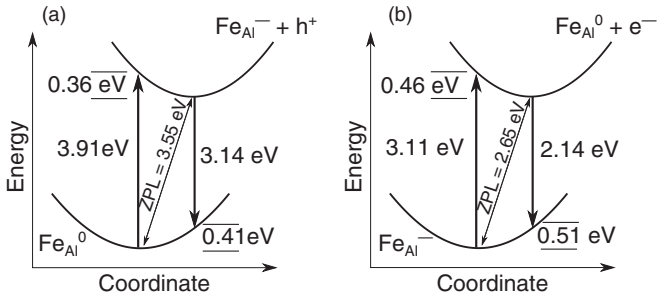

FIG. 12. Configuration-coordinate diagrams for the Fe_{Al} impurity in AlN. (a) A transition between the $(0/-)$ level and a hole at the VBM leads to an absorption peak at 3.91 eV and emission at 3.14 eV. (b) A transition between the $(0/-)$ level and an electron at the CBM leads to an emission peak at 2.14 eV.

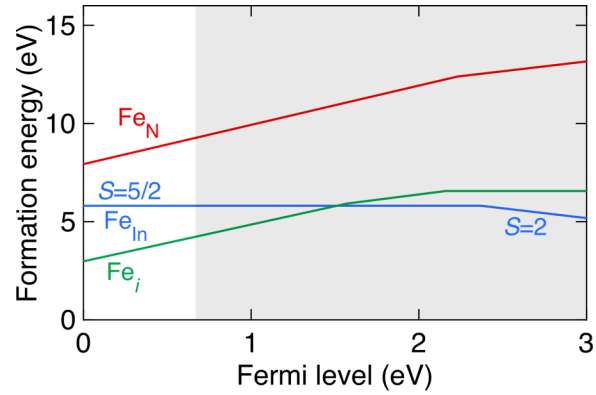

FIG. 13. Formation energy vs Fermi level for Fe_{In}, Fe_N, and Fe_i in InN in different charge states under In-rich conditions. The shaded area indicates energies above the CBM of InN.

excited state of Fe^0_{Al} in AlN. This value is almost identical to the energy difference between the $S = 5/2$ ground state and the first $S = 3/2$ excited state for Fe^0_{Ga} in GaN, confirming the conclusion that Fe^0_{Ga} and Fe^0_{Al} exhibit very similar optical transitions.

V. IRON IMPURITIES IN InN

The formation energies for various configurations of Fe in InN are illustrated in Fig. 13. Since the formation enthalpy of InN is very small, only minor differences occur between the formation energies under In-rich and N-rich conditions; hence, we present results only for In-rich conditions. In Fig. 13 we allow for the fact that the Fermi level may be well above the CBM in InN; indeed, while the band gap of InN is small, the material can be highly doped and has a small conduction-band density of states, which can push the Fermi level well above the CBM [70].

Fe incorporated on the In site, Fe_{In}, is stable in the neutral charge state across the entire InN band gap and assumes a high-spin configuration as a spin sextuplet ($S = 5/2$). The transition to the negative charge state occurs only at 1.69 eV above the CBM (2.37 eV above the InN VBM) and will probably never be reached. In the neutral charge state, the nearest-neighbor nitrogen atoms relax inwards by 8.2% of the In-N bond length. We find the occupied Fe d spin-up states to be located below the InN valence band, 6.5 eV below the VBM. The corresponding unoccupied Fe d spin-down states are located 2.9 eV above the InN CBM. Unlike GaN and AlN, we do not find the positive charge state of Fe_{In} to be stable; this is likely due to the VBM of InN being higher than that of GaN (and AlN), as discussed below. The first excited state of Fe^0_{In} (a quadruplet) could not be converged using the ΔSCF approach; for this reason we do not discuss the excited-state properties of Fe_{In}. Also, the low band gap of InN (0.68 eV) precludes optical transitions in the visible.

The incorporation of Fe on the N site in the 2+ charge state, Fe^{2+}_N, results in a large axial displacement of the Fe atom and an outward displacement of the nearest-neighbor In atoms. The in-plane Fe-In bond lengths are 23% larger than the equilibrium In-N bond lengths, while the axial Fe-In bond length is 17% larger. Fe_N acts as a double donor, and

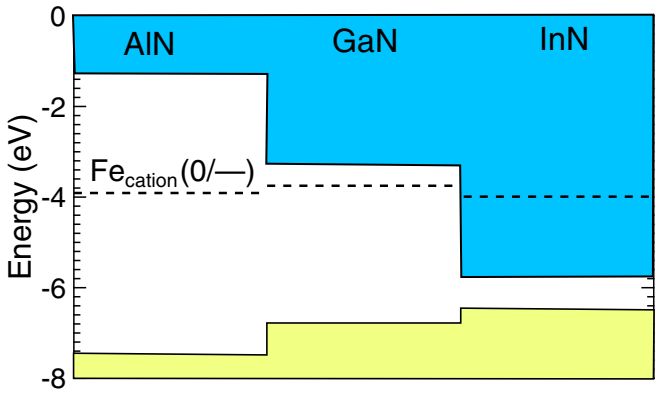

FIG. 14. Charge-state transition levels of Fe on the cation site (Ga, Al, In) in GaN, AlN, and InN. The $(0/-)$ acceptor levels associated with Fe substituted on the cation sites are plotted as dotted lines. The band structures are aligned according to Ref. [72]. The zero of energy corresponds to the vacuum level.

since the $(2+/+)$ level occurs well above the CBM, it would contribute two electrons to the CBM, i.e., it would act as a shallow double donor. However, its formation energy is high and hence it is unlikely to occur.

A major difference compared to GaN occurs for the iron interstitial: Fe_i is lower in energy than Fe_{In} for Fermi levels within the band gap and well into the conduction band. The lower energy can be attributed to the larger lattice parameters of InN, which favor incorporation on an interstitial site. Fe_i is stable in the $2+$ charge state across the InN band gap. A $(2+/+)$ transition level occurs at 0.77 eV above the CBM and a $(+/0)$ level at 1.46 eV above the CBM. Our results thus indicate that Fe_i in InN acts as a shallow donor.

VI. TRENDS DUE TO THE INCORPORATION OF Fe IN GaN, AlN, AND InN

In 1985, Langer and Heinrich [71] proposed that transition-metal impurity levels would align on a common energy scale, i.e., when the band structures of host materials were aligned according to the band offsets between them. It is instructive to check if this rule applies to the Fe_{cation} $(0/-)$ level in the III-nitrides. Using the band alignments between the III-nitrides determined based on another alignment method [using the $(+/-)$ level of interstitial hydrogen [72], we plot the $(0/-)$ level of Fe incorporated on the cation site of each material in Fig. 14. The $(0/-)$ levels turn out to be aligned within 0.33 eV. If we would use the slightly different band offsets from Ref. [73], the $(0/-)$ levels would be aligned to within 0.22 eV.

We build further understanding and analyze the trends associated with incorporating Fe in the III-nitrides by comparing the formation energies for all three materials in Fig. 15. We find that incorporation of Fe on the N site is unfavorable in each of the materials. This can be attributed to the large mismatch in ionic radii between Fe and N across all three materials. Indeed, we find the incorporation of Fe on the N site to lead to large, asymmetric relaxations of the nearest-neighbor Fe-cation bond lengths.

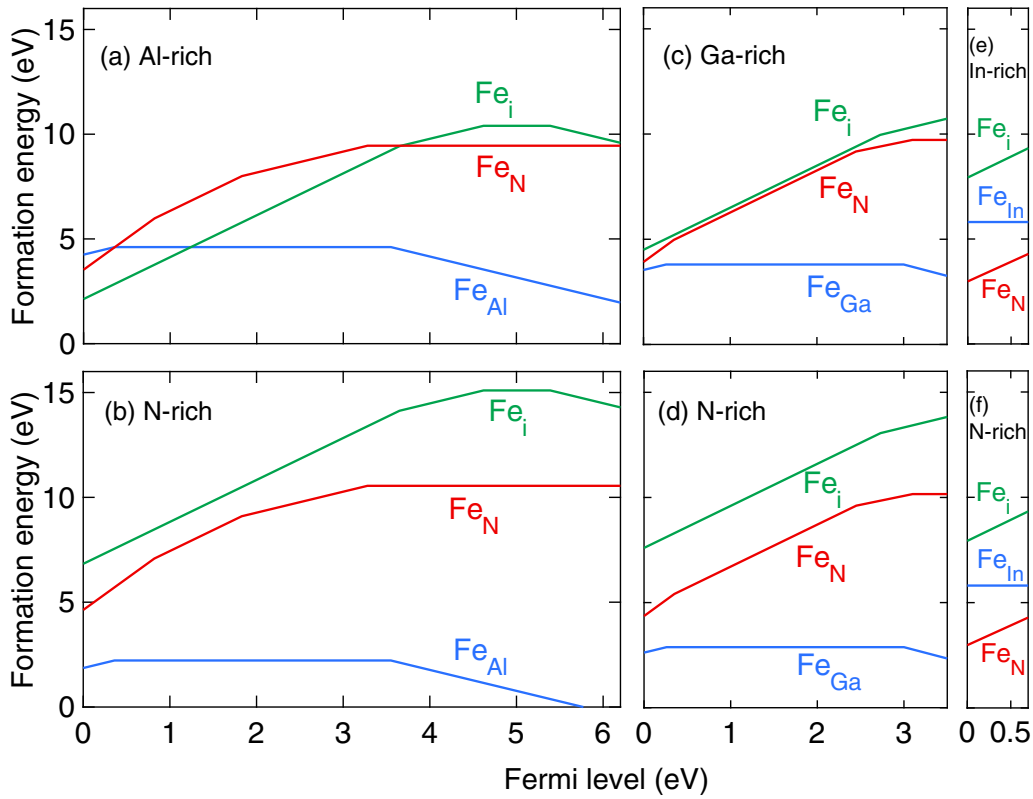

FIG. 15. Comparison of formation energies for Fe incorporated on cation (blue) or nitrogen sites (red) and as an interstitial (green). (a, b) Results for AlN, (c, d) for GaN, and (e, f) for InN under cation- and nitrogen-rich conditions.

In contrast, the incorporation of Fe on the cation site leads to significantly smaller structural relaxations. The ionic radius of Fe in the 3+ oxidation state is 0.49 Å. For comparison, the ionic radius is 0.39 Å for Al, 0.47 Å for Ga, and 0.62 Å for In. The mismatch in ionic radii is thus smallest in GaN and larger in AlN and InN. To understand the trends in formation energies across all three compounds, we need to take into account that the formation energies of Fe_{cation} also depend on the chemical potentials. For N-rich conditions at the solubility limit (set by Fe_3N), the formation energies [cf. Eq. (1)] contain a term ΔH_f, the formation enthalpy of the host material. This chemical-potential trend counteracts the size trend between AlN and GaN but adds to the formation energy difference for Fe_{cation} between GaN and InN.

The trends for incorporation of Fe as an interstitial finally can be understood mainly on the basis of atomic size: the larger lattice spacing in InN leads to lower formation energies in InN compared to GaN and AlN.

VII. SUMMARY AND CONCLUSIONS

Using hybrid functional first-principles calculations, we have investigated the electrical and optical properties of iron impurities and their complexes in GaN, AlN, and InN. Results for the formation energies of Fe incorporated in each material are summarized in Fig. 15. We find that iron incorporated substitutionally on the cation site in GaN and AlN acts as a deep acceptor and gives rise to optical absorption and emission in the visible or UV, as well as intradefect transitions in the IR. The excited states associated with the *d*-state manifold also play an important role in nonradiative recombination. In InN, Fe_i acts as a shallow double donor. We also examined the formation of complexes of Fe in GaN with native defects and impurities, finding that Fe_{Ga}-O_N is most likely to form. We suggest that Fe_{Ga} (and not a complex) is the cause of current collapse in AlGaN/GaN HEMTs. Our results allow us to provide consistent explanations for the observed optical transitions (both free-to-bound and internal transitions) and address the competition between radiative and nonradiative recombination.

ACKNOWLEDGMENTS

We gratefully acknowledge insightful discussions with Georg Kresse. This work was supported by the U.S. Department of Energy (DOE), Office of Science, Basic Energy Sciences (BES) under Award No. DE-SC0010689. D.W. was supported in part by a National Research Council (NRC) fellowship at the US Naval Research Laboratory. Work by A.A. was supported by the American Physical Society through the International Research Travel Award Program (IRTAP). The Flatiron Institute is a division of the Simons Foundation. Computational resources were provided by the National Energy Research Scientific Computing Center (NERSC), a U.S. Department of Energy, Office of Science User Facility operated under Contract No. DE-AC02-05CH11231.

[1] S. Nakamura and M. R. Krames, Proc. IEEE **101**, 2211 (2013).
[2] S. Chowdhury and U. K. Mishra, IEEE Trans. Electron Devices **60**, 3060 (2013).
[3] J. Freitas, M. Gowda, J. Tischler, J.-H. Kim, L. Liu, and D. Hanser, J. Cryst. Growth **310**, 3968 (2008).
[4] T. Dietl and H. Ohno, Rev. Mod. Phys. **86**, 187 (2014).
[5] A. Twardowski, J. Appl. Phys. **67**, 5108 (1990).
[6] A. Bonanni, M. Kiecana, C. Simbrunner, T. Li, M. Sawicki, M. Wegscheider, M. Quast, H. Przybylińska, A. Navarro-Quezada, R. Jakieła, A. Wolos, W. Jantsch, and T. Dietl, Phys. Rev. B **75**, 125210 (2007).
[7] J. B. Varley, A. Janotti, and C. G. Van de Walle, Phys. Rev. B **93**, 161201(R) (2016).
[8] J. Baur, K. Maier, M. Kunzer, U. Kaufmann, J. Schneider, H. Amano, I. Akasaki, T. Detchprohm, and K. Hiramatsu, Appl. Phys. Lett. **64**, 857 (1994).
[9] S. Leone, F. Benkhelifa, L. Kirste, C. Manz, S. Mueller, R. Quay, and T. Stadelmann, Phys. Status Solidi B **255**, 1700377 (2018).
[10] M. E. Zvanut, J. Dashdorj, J. A. Freitas, E. R. Glaser, W. R. Willoughby, J. H. Leach, and K. Udwary, J. Electron. Mater. **45**, 2692 (2016).
[11] M. Iwinska, R. Piotrzkowski, E. Litwin-Staszewska, V. Y. Ivanov, H. Teisseyre, M. Amilusik, B. Lucznik, M. Fijalkowski, T. Sochacki, N. Takekawa, H. Murakami, and M. Bockowski, J. Cryst. Growth **475**, 121 (2017).
[12] V. Shenai-Khatkhate and S. J. Manzik, US Patent No. 20140061956 (2015).
[13] V. Desmaris, M. Rudzinski, N. Rorsman, P. Hageman, P. Larsen, H. Zirath, T. Rodle, and H. Jos, IEEE Trans. Electron Devices **53**, 2413 (2006).
[14] T. Uždavinys, S. Marcinkevičius, J. Leach, K. Evans, and D. Look, J. Appl. Phys. **119**, 215706 (2016).
[15] Y. Fang, X. Wu, J. Yang, Z. Xiao, Y. Yang, F. Zhou, and Y. Song, Appl. Phys. Lett. **107**, 051901 (2015).
[16] J. Baur, K. Maier, M. Kunzer, U. Kaufmann, and J. Schneider, Appl. Phys. Lett. **65**, 2211 (1994).
[17] L. Jiang, S. Jin, W. Wang, S. Zuo, Z. Li, S. Wang, K. Zhu, Z. Wei, and X. Chen, Sci. Rep. **5**, 17979 (2015).
[18] K. Pressel, R. Heitz, S. Nilsson, P. Thurian, A. Hoffmann, and B. Meyer, Mater. Res. Soc. Symp. Proc. **395**, 613 (1995).
[19] X. Ji, S. Lau, S. Yu, H. Yang, T. Herng, A. Sedhain, J. Lin, H. Jiang, K. Teng, and J. Chen, Appl. Phys. Lett. **90**, 193118 (2007).
[20] H. Li, G. Cai, and W. Wang, AIP Adv. **6**, 065025 (2016).
[21] E. Malguth, A. Hoffmann, and M. R. Phillips, Phys. Status Solidi B **245**, 455 (2008).
[22] D. Wickramaratne, J.-X. Shen, C. E. Dreyer, M. Engel, M. Marsman, G. Kresse, S. Marcinkevičius, A. Alkauskas, and C. G. Van de Walle, Appl. Phys. Lett. **109**, 162107 (2016).
[23] A. Alkauskas, C. E. Dreyer, J. L. Lyons, and C. G. Van de Walle, Phys. Rev. B **93**, 201304(R) (2016).
[24] G. M. Dalpian, J. L. F. Da Silva, and S.-H. Wei, Phys. Rev. B **79**, 241201(R) (2009).

[25] X. Y. Cui, B. Delley, A. J. Freeman, and C. Stampfl, Phys. Rev. Lett. **97**, 016402 (2006).

[26] U. Gerstmann, A. T. Blumenau, and H. Overhof, Phys. Rev. B **63**, 075204 (2001).

[27] C. Freysoldt, B. Grabowski, T. Hickel, J. Neugebauer, G. Kresse, A. Janotti, and C. G. Van de Walle, Rev. Mod. Phys. **86**, 253 (2014).

[28] A. Alkauskas and A. Pasquarello, Phys. Rev. B **84**, 125206 (2011).

[29] T. Zakrzewski and P. Boguslawski, J. Alloy Compd. **664**, 565 (2016).

[30] A. Stroppa, G. Kresse, and A. Continenza, Phys. Rev. B **83**, 085201 (2011).

[31] A. Stroppa and G. Kresse, Phys. Rev. B **79**, 201201(R) (2009).

[32] Y. Puzyrev, R. Schrimpf, D. Fleetwood, and S. Pantelides, Appl. Phys. Lett. **106**, 053505 (2015).

[33] A. Polyakov, N. Smirnov, A. Govorkov, N. Pashkova, A. Shlensky, S. Pearton, M. Overberg, C. Abernathy, J. Zavada, and R. Wilson, J. Appl. Phys. **93**, 5388 (2003).

[34] Q. Yan, A. Janotti, M. Scheffler, and C. G. Van de Walle, Appl. Phys. Lett. **100**, 142110 (2012).

[35] J. Neugebauer and C. G. Van de Walle, Appl. Phys. Lett. **69**, 503 (1996).

[36] C. G. Van de Walle and J. Neugebauer, Annu. Rev. Mater. Res. **36**, 179 (2006).

[37] J. Heyd, G. E. Scuseria, and M. Ernzerhof, J. Chem. Phys. **118**, 8207 (2003).

[38] G. Kresse and J. Hafner, Phys. Rev. B **47**, 558 (1993).

[39] G. Kresse and J. Furthmüller, Phys. Rev. B **54**, 11169 (1996).

[40] J. L. Lyons, A. Janotti, and C. G. Van de Walle, Phys. Rev. B **89**, 035204 (2014).

[41] O. Madelung, *Semiconductors—Basic Data* (Springer Science & Business Media, New York, 2012).

[42] P. E. Blöchl, Phys. Rev. B **50**, 17953 (1994).

[43] C. Freysoldt, J. Neugebauer, and C. G. Van de Walle, Phys. Status Solidi B **248**, 1067 (2011).

[44] C. Freysoldt, J. Neugebauer, and C. G. Van de Walle, Phys. Rev. Lett. **102**, 016402 (2009).

[45] A. Stoneham, Philos. Mag. **36**, 983 (1977).

[46] A. Alkauskas, M. D. McCluskey, and C. G. Van de Walle, J. Appl. Phys. **119**, 181101 (2016).

[47] J. Dashdorj, M. Zvanut, J. Harrison, K. Udwary, and T. Paskova, J. Appl. Phys. **112**, 013712 (2012).

[48] P. Alippi, F. Filippone, G. Mattioli, A. A. Bonapasta, and V. Fiorentini, Phys. Rev. B **84**, 033201 (2011).

[49] H. Raebiger, S. Bae, C. Echeverría-Arrondo, and A. Ayuela, Phys. Rev. Mater. **2**, 024402 (2018).

[50] D. Dumcenco, S. Levcenco, Y. Huang, C. Reynolds, Jr., J. Reynolds, K. Tiong, T. Paskova, and K. Evans, J. Appl. Phys. **109**, 123508 (2011).

[51] B. Neuschl, M. Gödecke, K. Thonke, F. Lipski, M. Klein, F. Scholz, and M. Feneberg, J. Appl. Phys. **118**, 215705 (2015).

[52] C. Wetzel, D. Volm, B. Meyer, K. Pressel, S. Nilsson, E. Mokhov, and P. Baranov, Appl. Phys. Lett. **65**, 1033 (1994).

[53] R. Heitz, P. Thurian, I. Loa, L. Eckey, A. Hoffmann, I. Broser, K. Pressel, B. Meyer, and E. Mokhov, Appl. Phys. Lett. **67**, 2822 (1995).

[54] R. O. Jones and O. Gunnarsson, Rev. Mod. Phys. **61**, 689 (1989).

[55] U. von Barth, Phys. Rev. A **20**, 1693 (1979).

[56] P. Thurian, A. Hoffmann, L. Eckey, P. Maxim, R. Heitz, I. Broser, K. Pressel, B. Meyer, J. Schneider, J. Baur, and M. Kunzer, Mater. Res. Soc. Symp. Proc. **449**, 707 (1996).

[57] P. Muret, J. Pernot, M. Azize, and Z. Bougrioua, J. Appl. Phys. **102**, 053701 (2007).

[58] N. G. Szwacki, J. A. Majewski, and T. Dietl, Phys. Rev. B **83**, 184417 (2011).

[59] F. Filippone, G. Mattioli, P. Alippi, and A. A. Bonapasta, Phys. Rev. Lett. **107**, 196401 (2011).

[60] M. Silvestri, M. J. Uren, and M. Kuball, Appl. Phys. Lett. **102**, 073501 (2013).

[61] H. Cho, K. Kim, C.-H. Hong, and H. Lee, J. Cryst. Growth **223**, 38 (2001).

[62] J. L. Lyons and C. G. Van de Walle, NPJ Comput. Mater. **3**, 12 (2017).

[63] M. Meneghini, I. Rossetto, D. Bisi, A. Stocco, A. Cester, G. Meneghesso, E. Zanoni, A. Chini, A. Pantellini, and C. Lanzieri, in *2014 IEEE International Reliability Physics Symposium,* (IEEE, New York, 2014), pp. 6C–6.

[64] S. Mukherjee, Y. Puzyrev, J. Chen, D. M. Fleetwood, R. D. Schrimpf, and S. T. Pantelides, IEEE Trans. Electron Devices **63**, 1486 (2016).

[65] A. Hierro, S. Ringel, M. Hansen, J. Speck, U. Mishra, and S. DenBaars, Appl. Phys. Lett. **77**, 1499 (2000).

[66] A. Alkauskas, Q. Yan, and C. G. Van de Walle, Phys. Rev. B **90**, 075202 (2014).

[67] C. Stampfl and C. G. Van de Walle, Appl. Phys. Lett. **72**, 459 (1998).

[68] H. Masenda, D. Naidoo, K. Bharuth-Ram, H. Gunnlaugsson, K. Johnston, R. Mantovan, T. Mølholt, M. Ncube, S. Shayestehaminzadeh, H. Gíslason, G. Langouche, S. Olafsson, and G. Weyer, J. Magn. Magn. Mater. **401**, 1130 (2016).

[69] V. Soltamov, I. Ilyin, A. Soltamova, E. Mokhov, and P. Baranov, J. Appl. Phys. **107**, 113515 (2010).

[70] A. Janotti, J. Lyons, and C. Van de Walle, Phys. Status Solidi A **209**, 65 (2012).

[71] J. M. Langer and H. Heinrich, Phys. Rev. Lett. **55**, 1414 (1985).

[72] C. G. Van de Walle and J. Neugebauer, Nature (London) **423**, 626 (2003).

[73] P. G. Moses, M. Miao, Q. Yan, and C. G. Van de Walle, J. Chem. Phys. **134**, 084703 (2011).